

Twisted magnetosphere with quadrupolar fields in the exterior of a neutron star

Yasufumi Kojima ^{*}

Department of Physics, Hiroshima University, Higashi-Hiroshima, Hiroshima 739-8526, Japan

6 November 2018

ABSTRACT

The magnetar magnetosphere is gradually twisted by shearing from footpoint motion, and stored magnetic energy also increases at the same time. When a state exceeds a threshold, flares/outbursts manifest themselves as a result of a catastrophic transition. Axisymmetric static solutions for a relativistic force-free magnetosphere with dipole–quadrupole mixed fields at the surface have been calculated. The quadrupole component represents a kind of magnetic-field irregularity at a small scale. Locally twisted models are constructed by limiting current flow regions, where the small part originates from a dipole–quadrupole mixture. The energy along a sequence of equilibria increases and becomes sufficient to open the magnetic field in some models. In energetically metastable states, a magnetic flux rope is formed in the vicinity of the star. The excess energy may be ejected as a magnetar flare/outburst. The general relativistic gravity is sufficient to confine the flux rope and to store huge magnetic energy, and the mechanism is also discussed.

Key words: stars: magnetars – stars: neutron – stars: magnetic fields

1 INTRODUCTION

Magnetars are a class of neutron stars with extremely strong magnetic fields. Their activities, such as sudden flares/bursts and persistent X-ray emissions, are powered by magnetic fields (e.g., [Turolla et al. 2015](#); [Kaspi & Beloborodov 2017](#), for a review). The interior magnetic field structure is never permanently fixed, but decays into heat on a secular timescale. The ohmic dissipation timescale for a global field structure is too long among possible mechanisms for this evolution. Therefore, other mechanisms e.g., Hall drift, ambipolar diffusion, or their combinations, are relevant. For example, the magnetic field drifts to be localized to a certain region in which ohmic dissipation is effectively enhanced. The evolutionary timescales for Hall drift and ambipolar diffusion are proportional to B and B^2 , where B is typical magnetic-field strength ([Goldreich & Reisenegger 1992](#)). These mechanisms may therefore be relevant to neutron stars with strong fields, e.g., $B > 10^{14}$ G. The magnetic fields for typical pulsars with $B \sim 10^{12}$ G are almost unchanged by them.

Among the other factors, magnetic field evolution has been extensively simulated under Hall drift in neutron-star crusts (e.g., [Hollerbach & Rüdiger 2004](#); [Kojima & Kisaka 2012](#); [Viganò et al. 2013](#); [Gourgouliatos & Cumming 2014](#); [Wood & Hollerbach 2015](#)). For example, [Geppert & Viganò \(2014\)](#) calculated the evolution in axially symmetric configuration, together with thermal evolution. Their magneto-thermal simulation shows a remarkable feature – a magnetic spot caused by an initially confined toroidal component that manifests itself on the surface around 10^4 years. Furthermore, [Gourgouliatos et al. \(2016\)](#) extended the Hall-magnetohydrodynamic simulation to a three-dimensional configuration and showed intense magnetic features at small-scales are driven by non-axially symmetric instabilities. Thus, higher multi-poles are likely to be produced via nonlinear coupling between poloidal and toroidal fields in the crust. There remain subtle problems concerning dependence of the initial magnetic geometries and the external fields. Such evolutions have been calculated in most previous research under the assumption that the exterior is in vacuum. Hall drift of magnetic field lines build up stresses in the crust, and shearing motion at the stellar surface twists the exterior magnetic field, irrespective of whether the neutron star crust responds to the magnetic stress elastically or plastically. The twisted structure is supported by flowing currents. When the state exceeds a threshold,

* E-mail: ykojima-phys@hiroshima-u.ac.jp

the energy is abruptly released on a much shorter dynamical timescale, leading to energetic flares. It is important to take into account the effect of the twisted magnetosphere instead of vacuum on the evolution. Recently, [Akgün et al. \(2017\)](#) modeled this evolution by taking into account the force-free magnetosphere. Their evolution model shows that there is no equilibrium solution for the exterior magnetosphere on timescales of the order of thousands of years. The breakdown of models at that time suggests an outburst. Subsequent evolution after the burst is not followed, as the rearrangement of magnetic fields cannot be calculated. Their initial configuration is simplified as a bipolar one, and there is not enough time for a transition to higher multi-pole states.

Static equilibrium solutions are helpful for understanding the magnetar magnetosphere. The force-free approximation may be applicable, since magnetospheres are filled by low-density plasma. Important elements involved in magnetar magnetospheres have been studied in the static approach. For example, twisted force-free magnetospheres around magnetars have been numerically constructed as a part of entire magnetic field structures from stellar cores to exteriors ([Glampedakis et al. 2014](#); [Fujisawa & Kisaka 2014](#); [Pili et al. 2015, 2017](#)). [Akgün et al. \(2016\)](#) studied the effect of a surrounding current-free region on a twisted magnetosphere. One of the interesting properties found in some numerical results is the formation of a magnetic flux rope, an axially symmetric torus in the vicinity of the stellar surface, when the magnetic field is highly twisted. The topology in the presence of the rope differs from that of the current-free potential field. There are multiple force-free solutions under fixed boundary conditions, and a higher state containing the flux rope is obtained by changing the iteration scheme to solve a non-linear Grad–Shafranov equation ([Akgün et al. 2018](#)).

The spacetime outside the magnetar is assumed to be flat except in a few studies ([Pili et al. 2015, 2017](#); [Kojima 2017](#); [Kojima & Okamoto 2018](#)). Treatment in flat spacetime seems to be reasonable as the lowest order approximation; a priori, the correction is expected to be not so large, since the relativistic factor is of order $G_N M / (Rc^2) \sim 0.2 - 0.3$ in neutron stars. In our previous studies ([Kojima 2017](#); [Kojima & Okamoto 2018](#)), however, we found that general relativistic effects are noteworthy. The maximum energy stored in a current-flowing relativistic magnetosphere increases by 132 percent from the current free dipole one. This contrasts with the maximum excess energy of only 34 percent in a non-relativistic model. This large increase in a relativistic model is related to the formation of a flux rope, an axially symmetric torus in the vicinity of the stellar surface, when the magnetic field structure is highly twisted. Curved spacetime helps to confine the torus.

It is reasonable to infer that near the magnetar surface, the magnetic field geometry involves higher multi-poles. Active regions manifest themselves as multi-polar regions. Therefore, our previous calculations are further extended to examine the effect of a higher multi-pole in this study. By considering a mixed dipole and quadrupole configuration at the surface, a locally twisted model is constructed. Relevant amounts of energy should be reduced by limiting the current flow region in the vicinity of a neutron star. This energy that comes from non-potential magnetic fields is available for rapid release through a variety of mechanisms that may involve instabilities, loss of equilibrium, and/or reconnection. When a detached magnetic flux is ejected, the structure becomes temporarily open. The structural change to an open field configuration is therefore impossible with respect to energy, from a state with energy stored in the magnetosphere exceeding open field energy. Our concern is whether or not the stored energy exceeds open field energy in the presence of multi-pole fields.

This study is organized as follows. We briefly discuss our model and relevant equations for a non-rotating force-free magnetosphere in a Schwarzschild spacetime in Section 2. We then numerically solve the so-called Grad–Shafranov equation assuming that the current function is given by a simple power-law model. In Section 3, the results are given for comparison with those obtained in flat spacetime. Finally, Section 4 summarizes and discusses the implications of our results. We use geometrical units of $c = G_N = 1$.

2 EQUATIONS

2.1 Force-free magnetosphere in a curved spacetime

In this section, we briefly summarize our formalism by vector analysis in curvilinear coordinates (see [Kojima 2017](#), for details). We consider the static magnetic configuration for the exterior of a non-rotating compact object with a mass M and radius R . The spacetime is described by the Schwarzschild metric for $R > 2M$. The magnetic field for the axially symmetric case is described by two functions G and S :

$$\vec{B} = \vec{\nabla} \times \left(\frac{G}{\varpi} \vec{e}_{\hat{\phi}} \right) + \frac{S}{\alpha\varpi} \vec{e}_{\hat{\phi}} = \frac{\vec{\nabla}G \times \vec{e}_{\hat{\phi}}}{\varpi} + \frac{S}{\alpha\varpi} \vec{e}_{\hat{\phi}}, \quad (1)$$

and its components can be written as

$$[B_{\hat{r}}, B_{\hat{\theta}}, B_{\hat{\phi}}] = \left[\frac{G_{,\theta}}{r\varpi}, -\frac{\alpha G_{,r}}{\varpi}, \frac{S}{\alpha\varpi} \right], \quad (2)$$

where $\alpha = (1 - 2M/r)^{1/2}$ and $\varpi = r \sin \theta$. The magnetic flux function G describes poloidal magnetic fields, and function S describes poloidal current flow as $4\pi\alpha\vec{j}_p = \vec{\nabla} \times (\alpha\vec{B}) = \vec{\nabla}S \times \vec{e}_{\hat{\phi}}/\varpi$. In a force-free approximation, the current flows along

magnetic field lines, and the current function S should be a function of G . We consider a specific power-law model with a positive constant γ :

$$S = \left(\frac{\gamma}{3}\right)^{1/2} G^3, \quad (3)$$

such that the current is simply given by

$$4\pi\alpha\vec{j} = (3\gamma)^{1/2}G^2\vec{B}. \quad (4)$$

In this model, the current always flows in the same direction as the magnetic field. The current distribution is weighted in favor of large $|G|$ values, such that the current is likely to be localized. The global structure of the magnetic field is determined by solving the azimuthal component of the Biot–Savart equation with current $j_{\hat{\phi}}$:

$$\frac{\varpi}{\alpha}\vec{\nabla} \cdot \left(\frac{\alpha}{\varpi^2}\vec{\nabla}G\right) = -4\pi j_{\hat{\phi}}. \quad (5)$$

The left hand side of this equation is explicitly written as

$$\frac{1}{\varpi} \left[\frac{\partial}{\partial r} \left(\alpha^2 \frac{\partial G}{\partial r} \right) + \frac{\sin\theta}{r^2} \frac{\partial}{\partial\theta} \left(\frac{1}{\sin\theta} \frac{\partial G}{\partial\theta} \right) \right], \quad (6)$$

and the source term of eq.(5) is simply reduced to $-\gamma G^5/(\alpha^2\varpi)$ [power-law model with $n = 5$ in (Flyer et al. 2004; Kojima 2017)].

It is instructive to rewrite eq.(5) as

$$\varpi\vec{\nabla} \cdot \left(\frac{1}{\varpi^2}\vec{\nabla}G\right) = -4\pi(j_{\hat{\phi}} + j_g), \quad (7)$$

where

$$4\pi j_g \equiv \frac{1}{\varpi}\vec{\nabla} \ln\alpha \cdot \vec{\nabla}G = -\frac{1}{\varpi}\vec{g} \cdot \vec{\nabla}G. \quad (8)$$

A new term j_g in eq.(7) arises from gravitational acceleration $\vec{g} = -\vec{\nabla} \ln\alpha$ in general relativity. It is ignored in treatment for flat spacetime. Indeed, the magnitude of j_g is not so large, as $M/R \approx 0.2$ times a true current. However, the 'general-relativity-induced current' j_g plays an important role on the confinement of a flux rope, as will be discussed in the next section.

2.2 Mixture of dipole and quadrupole

It is useful to show analytic solutions in vacuum, for eq.(5) with $\vec{j} = 0$. The magnetic function G is expanded using Legendre polynomials $P_l(\theta)$:

$$G(r, \theta) = -\sum_{l \geq 1} g_l(r) \sin\theta \frac{dP_l(\theta)}{d\theta}. \quad (9)$$

The radial functions g_l are for example given by (e.g. Pétri 2017, for higher l)

$$\begin{aligned} g_1 &= -\frac{3B_0R^3r^2}{8M^3} \left[\ln\left(1 - \frac{2M}{r}\right) + \frac{2M}{r} + \frac{2M^2}{r^2} \right] \\ &\approx \frac{B_0R^3}{r} \left[1 + \frac{3M}{2r} + \frac{12M^2}{5r^2} + \dots \right], \quad (M/r \ll 1) \end{aligned} \quad (10)$$

$$\begin{aligned} g_2 &= -\frac{5B_0R^4r^3}{2M^5} \left[\left(1 - \frac{3M}{2r}\right) \ln\left(1 - \frac{2M}{r}\right) + \frac{M}{r} \left(2 - \frac{M}{r} - \frac{M^2}{3r^2}\right) \right] \\ &\approx \frac{B_0R^4}{r^2} \left[1 + \frac{8M}{3r} + \frac{40M^2}{7r^2} + \dots \right], \quad (M/r \ll 1) \end{aligned} \quad (11)$$

where B_0 is typical field strength and R is the stellar surface radius. In these expressions, the first expression is an exact solution, and the second is its approximation under the weak gravity regime $M/r \ll 1$. Multi-pole moments are generally defined by the asymptotic form approaching infinity. For example, the magnetic dipole moment μ is given by $\mu = B_0R^3$. The surface magnetic field strength B_p at magnetic polar cap is simply given by $B_p = 2B_0 = 2\mu/R^3$ in a flat spacetime model. However, it should be noted that additional relativistic corrections are needed to connect the surface field with B_0 in a curved spacetime model, and that the difference between g_l and a simple power-law solution ($\propto r^{-l}$) in a flat spacetime increases with l . Accordingly, the relativistic correction is more important in higher multi-poles. The function g_2 in eq.(11) is also normalized by the same constant B_0 .

We solve the non-linear equation (5) using a numerical method described in Kojima (2017). Here, we discuss the boundary conditions. At the polar axis, the magnetic function G should satisfy the regularity condition, that is, $G = 0$ at $\theta = 0$ and π . At asymptotic infinity ($r \rightarrow \infty$), the function should decrease as $G \propto r^{-1}$. At the stellar surface $r = R$, the function

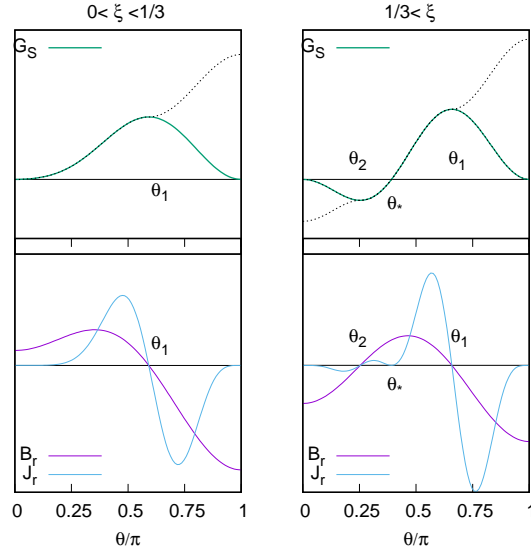


Figure 1. Magnetic function G_S (top panel), radial component of magnetic field $B_{\hat{r}}$, and current $j_{\hat{r}}$ (bottom panel) at the surface as a function of polar angle θ . The vertical axis is arbitrary scaled. The left panels are for a dipole-dominated field with a parameter $0 < \xi < 1/3$, and the right panels are for a quadrupole-dominated field with $1/3 < \xi$. The function G_S becomes zero at a certain angle θ_* ($0 < \theta_* < \pi$) in the latter. Zeros of $B_{\hat{r}} = 0$ at the surface are denoted in the figure as $\theta = \theta_n$ ($n = 1, 2$). In the top panels, a dotted line corresponds to a monopolar configuration.

$G_S(\theta) \equiv G(R, \theta)$ is assumed to be a mixture of dipole ($l = 1$) and quadrupole ($l = 2$) fields with a ratio a_2 ¹. The angular dependence is set by

$$\begin{aligned} G_S(\theta) &= - \left(g_1(R) \sin \theta \frac{dP_1(\theta)}{d\theta} - a_2 g_2(R) \sin \theta \frac{dP_2(\theta)}{d\theta} \right) \\ &= [g_1(R) - 3a_2 g_2(R) \cos \theta] \sin^2 \theta, \end{aligned} \quad (12)$$

where $g_l(R)$ ($l = 1, 2$) given in eqs. (10)-(11) are incorporated to determine the boundary value. For a fixed ratio a_2 and relativistic factor M/R , the solutions in vacuum are expressed simply by a sum of eqs. (10)-(11). The potential field configuration is used as a reference, and twisted magnetospheres are constructed by including toroidal magnetic field $B_{\hat{\phi}}$.

Figure 1 shows $G_S(\theta)$ in eq. (12). There are two cases that depend on a parameter $\xi \equiv a_2 g_2 / g_1$, which is simply reduced to the ratio a_2 in a flat spacetime. One is a dipole-like configuration when $0 \leq \xi < 1/3$, and the other is a quadrupole-like one when $\xi \geq 1/3$. In the latter, G_S becomes zero at an angle θ_* ($0 < \theta_* < \pi/2$). Figure 1 also shows the radial component of magnetic field $B_{\hat{r}} \propto G_{S,\theta}$ and radial current $4\pi\alpha j_{\hat{r}} \propto G_S^2 B_{\hat{r}}$, where eqs. (2) and (4) are used. We denote the angles θ_n ($n = 1, 2$) as the root of $B_{\hat{r}} = 0$. The direction of $j_{\hat{r}}$ ($\propto B_{\hat{r}}$) changes at θ_1 in a dipole-dominated field ($0 \leq \xi < 1/3$), whereas it changes twice at θ_1 and θ_2 in a quadrupole-dominated field ($\xi \geq 1/3$).

In this paper, we consider two kinds of models by restricting the current-flowing region when the model (3) is applied. In the 'whole flowing-model', eq.(3) is applied everywhere, irrespective of the sign of G . The current flows in the magnetosphere along a constant line of G , inwards or outwards at the surface as shown in Fig.1. The toroidal field $B_{\hat{\phi}}$ is positive definite for the parameter $0 \leq \xi < 1/3$, whereas it changes the direction of a border line started from θ_* on the surface for $\xi \geq 1/3$. This current model provides a globally twisted magnetosphere. Another model is relevant to the quadrupole-like configuration only ($\xi \geq 1/3$). The current flowing region in the magnetosphere is limited by applying eq.(3) only to a smaller region with magnetic field lines starting from $0 < \theta < \theta_*$ ($< \pi/2$) on the surface, that is, a negative region of G . In this 'partially flowing-model', there is a small circuit started from $\theta_2 < \theta < \theta_*$, and back to the polar region $0 < \theta < \theta_2$ on the surface, as shown in Fig. 1. This model describes a locally twisted magnetosphere.

¹ We consider $a_2 > 0$ only, since $a_2 < 0$ corresponds to north-south inversion with respect to θ .

2.3 Helicity and energy

Two integrals, those of magnetic helicity and energy, are useful to characterize the equilibrium solution of the magnetospheres. Magnetic helicity represents a global property of magnetic fields, and is obtained by integrating the product of two vectors, namely, \vec{A} and $\vec{B}(=\nabla\times\vec{A})$. A quantity H_R , which can be defined by the difference between the magnetic helicity of the force-free field and that of the potential field with the same surface boundary condition. The total relative helicity in the exterior ($r\geq R$) is given by

$$H_R = 4\pi \int_{r\geq R} \frac{GS}{\alpha^2} \frac{drd\theta}{\sin\theta}. \quad (13)$$

Magnetic energy stored in the force-free magnetosphere is also given by integrating over the 3-dimensional volume:

$$E_{EM} = \frac{1}{4} \int_{r\geq R} \left[\left(\alpha \frac{\partial G}{\partial r} \right)^2 + \left(\frac{1}{r} \frac{\partial G}{\partial \theta} \right)^2 + \left(\frac{S}{\alpha} \right)^2 \right] \frac{drd\theta}{\sin\theta}. \quad (14)$$

The numerical results of H_R and E_{EM} , which depends on the twist, is given in the next section.

Here we discuss the energy for two reference configurations. One is given by that for the potential field for a given boundary condition (12). It corresponds to the lowest energy and is calculated in terms of solutions g_l ($l=1,2$) (eqs. (10)-(11)). The energy of a dipolar potential field is $E_d = B_0^2 R^3/3$, and that of a quadrupolar potential field is $E_q = 6B_0^2 R^3/5$ in flat spacetime. Their values for a relativistic model with $M/R = 0.25$ are numerically calculated as $E_d = 0.74B_0^2 R^3$ and $E_q = 5.14B_0^2 R^3$. When the boundary field is a dipole–quadrupole mixture with a ratio a_2 , the energy is given by $E_0 = E_d + a_2^2 E_q$. The potential energy of a quadrupole is larger than that of a dipole, when $a_2 \geq (E_d/E_q)^{1/2} \approx 0.4-0.5$, for the relativistic factor M/R .

Another important energy is E_{open} , which is energy stored in the open field with the same boundary condition (12). Suppose the initially closed magnetic field lines of a force-free magnetosphere are stretched out to infinity by some artificial means, keeping the same surface condition; energy is increased in the new state. When the energy E_{EM} of a force-free magnetosphere exceeds E_{open} , an open field configuration is preferable in energy. Such a state with $E_{EM} > E_{open}$ may be related to the abrupt transition with mass ejection.

Figure 2 schematically demonstrates the open field configuration. The quadrupole component is slightly larger than the dipolar one at the stellar surface, i.e., a case of $\xi > 1/3$. The surface condition of this example is described in the right panel of Fig. 1. Corresponding to the surface boundary condition, there are two families of closed field lines: They are either lines with $G > 0$ or those with $G < 0$. One of closed field lines becomes open under the partially open configuration, whereas both closed lines are open in a fully open configuration. In the latter, larger energy is associated with the transition. We only consider a partially open configuration in this paper. The middle panel of Fig. 2 shows the closed field lines of $G > 0$ are opened, and the right panel shows those of $G < 0$ are opened.

The method to calculate E_{open} is discussed by (e.g., Low & Smith 1993). Here, we briefly explain it to give an example in the case of $\xi > 1/3$. We modify the boundary condition (12) at the surface as

$$\begin{aligned} G_S^*(\theta) &= G_S(\theta) & (0 \leq \theta \leq \theta_1), \\ G_S^*(\theta) &= 2G_S^*(\theta_1) - G_S(\theta) & (\theta_1 < \theta \leq \pi). \end{aligned} \quad (15)$$

In the top panel of Fig.1, $G_S(\theta)$ is plotted by a solid line, and $G_S^*(\theta)$ by a dotted one. As inferred from the figure, it is necessary to contain the monopolar function $1 - \cos\theta$ to express $G_S(\theta)$. By solving eq.(5) with $S = 0$ and surface boundary condition $G_S(\theta)$, we have a quadrupolar potential field, which is shown in the left panel of Fig.2. By replacing it with $G_S^*(\theta)$, a partially open field solution G_{open} is obtained. All the field lines with $G > 0$ extend to infinity. The magnetic configuration is shown in the middle panel of Fig.2. The solution with $G_S^*(\theta)$ is unphysical since it contains a magnetic monopole charge. The desired solution is obtained by reversing its direction only on those lines starting from a region of $\theta_1 < \theta \leq \pi$ on the surface. The magnetic energy is unchanged by this sign-flipping, and may be calculated for the solution G_{open} . Here is a remark on the temporary transition of a twisted magnetosphere. A field line originating from polar angle θ_1 on the surface in Fig.2 corresponds to the current sheet, which separates regions of opposite magnetic polarity. The open field is strict poloidal, with $B_{\hat{\phi}} = 0$, although the force-free field is twisted with $B_{\hat{\phi}} \neq 0$. A finite twist is assumed to propagate to infinity along open field lines.

The same method is applied to opening closed lines starting from a region $0 < \theta < \theta_2$ on the surface in Fig.2, although it is enough to consider the boundary modification with respect to θ_1 in the case of $\xi < 1/3$. Partially open field energy is in general different with respect to the opening angle θ_n . The energy regarding θ_1 is larger than that for θ_2 .

3 NUMERICAL RESULTS

3.1 A sequence of solutions

A sequence of magnetospheres is numerically constructed for a fixed boundary condition with a ratio a_2 and a relativistic factor M/R . We start with a potential field solution, and follow the structure change by increasing the azimuthal magnetic

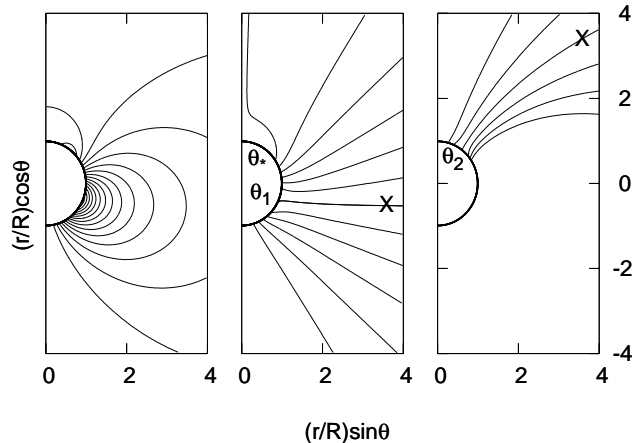


Figure 2. Magnetic field lines for a dipole–quadrupole mixture in the case of $\xi > 1/3$. The surface condition is given in the right panel of Fig. 1. The left panel shows the potential field lines. The middle and right panels show open field lines with the same surface condition. In the partially open configuration, the field lines with $G > 0$ are relevant to the opening. There are still closed lines originating from $0 < \theta < \theta_*$ on the surface, but they are not displayed in the middle panel for simplicity. The right panel shows partially open field lines with $G < 0$, and closed lines originating from $\theta_* < \theta < \pi$ are not displayed. The current sheet is located on a line with a \times symbol, although this is not necessary for this work.

flux or helicity, which is used as the degree of twist, and the constant γ is posteriorly determined. Thus, both magnetic energy E_{EM} and relative helicity H_{R} are multi-valued functions of γ . The increase in magnetic energy and the relative helicity for some examples are shown in Figs. 3 and 4. The results in flat spacetime ($M/R = 0$) are given in Fig. 3, and relativistic models ($M/R = 0.25$) are given in Fig. 4. Left and middle panels are results for a whole current-flowing model, while the right panel corresponds to those for a partially current-flowing model. For a better understanding of the mechanism, the energy difference $\Delta E (= E_{\text{EM}} - E_0)$ is divided into $\Delta E = \Delta E_t + \Delta E_p$, comprising that of the toroidal component and that of the poloidal component.

The general tendency is the same in all models. There are two branches in the curves of ΔE_p , ΔE_t and H_{R} , as functions of γ . In the lower branch, which corresponds to a weak toroidal magnetic field, the energy ΔE_t increases monotonically with the strength parameter γ . The helicity H_{R} also increases, but the poloidal energy is almost constant, $\Delta E_p \approx 0$. There is a maximum of γ , and after passing the turning point, ΔE_p drastically increases in the upper branch. This means a significant structural change from that in the potential field. This conclusion is confirmed later. The curve of ΔE_p or ΔE_t in Figs. 3 and 4 no longer increases, but curls into a limiting point by further twisting. This behavior is similar to that often appearing near a critical point in nonlinear dynamics. Flyer et al. (2004); Zhang et al. (2006, 2012) demonstrated the detailed behavior with the current model in a flat spacetime. A careful treatment is necessary by changing the parameter near the endpoint. In this research, we do not resolve the endpoint of the sequence, but the maximum value in energy or helicity is unchanged, even further exploring the termination.

The general property along the sequence is the same whether or not the relativistic effect is taken into account, but the maximum values of ΔE_p , ΔE_t , and H_{R} in Figs. 3 and 4 are quite different. We normalize the energy excess ΔE by potential field energy E_0 , which depends on magnetic field strength B_0 , a ratio a_2 , stellar radius R and relativistic factor M/R . The ratio $\Delta E_p/E_0$ or $\Delta E_t/E_0$ depends on a_2 and M/R , and clarify the effects of magnetic field configuration and general relativity. The maximum value by the relativistic treatment increases by a factor of 2 to 5 for fixed a_2 . This increase caused by curved space is already demonstrated for the model with $a_2 = 0$ (Kojima 2017).

3.2 Magnetic field configuration

We present the results of a flat spacetime treatment ($M/R = 0$). Figure 5 shows the magnetic function G with contour lines and toroidal magnetic field B_ϕ with colors in the r - θ plane. Only the interior part is shown, since the field in the exterior

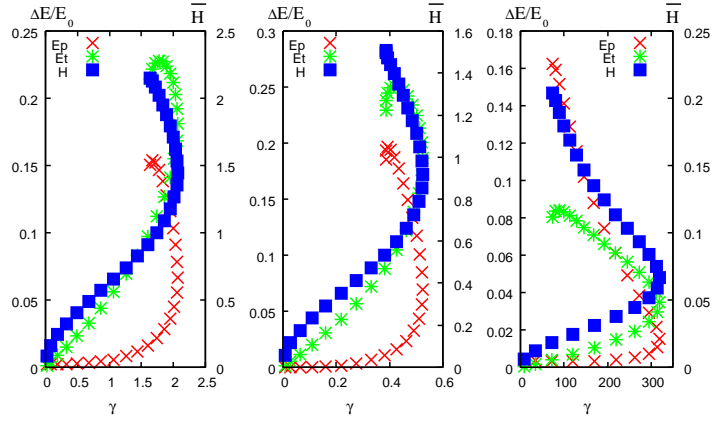


Figure 3. Increase in magnetic energy $\Delta E/E_0$ from the potential dipole field is shown on the left axis and total relative helicity $\bar{H} \equiv H_R/(4\pi E_0 R)$ is shown on the right axis. The poloidal component of the energy is denoted by crosses, the toroidal component by asterisks, and helicity by squares. The horizontal axis denotes the dimensionless value $\gamma B_0^4 R^{10}$. Results for the whole current-flowing model in a flat spacetime are shown in the left ($a_2 = 0.2$) and middle panels ($a_2 = 1$). The right panel ($a_2 = 1$) shows the results for a partially current-flowing model.

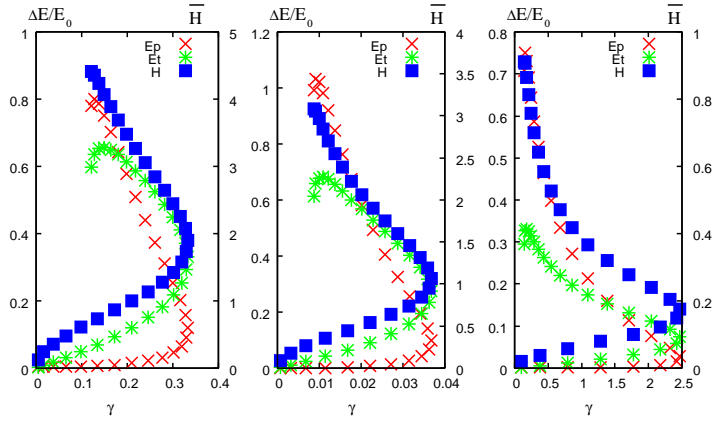


Figure 4. This figure reflects the same conditions as in Fig. 3, but for models with a relativistic factor $M/R = 0.25$.

approaches a vacuum solution since $S \propto G^3 \rightarrow 0$, and the outer part is unchanged. The surface field is given by a quadrupole dominated field with $a_2 = 1$. The left panel shows potential field ($B_{\hat{\phi}} = 0$), and the others show the structure for a highly twisted model. The middle panel shows the result of the whole flowing-model, and the right shows that for a partially flowing-model. They correspond to the end points along a sequence of middle and right panels in Fig. 3. In comparison with the potential field, magnetic lines are stretched outwards by a flowing current. The maximum of the toroidal field $B_{\hat{\phi}}$ is located at latitude $\theta \approx \theta_1$ in the middle panel. This is related to the maximum of the function $|G_S(\theta)|$ (eq.(12)) at surface, since $B_{\hat{\phi}} \propto G^3$ in our current model. The magnetic structure in the northern hemisphere is almost unchanged in a globally twisted model, since most current flow is confined to a region $\pi/2 < \theta \approx \theta_1 < \pi$. However, an elongated field structure appears in the northern hemisphere in a constrained current-flow model as shown in the right panel. Numerical results show that it is possible to sustain strong $B_{\hat{\phi}}$, and that a flux rope is formed. The center is located at $(r/R, \theta) \approx (1.5, \theta_2)$. Note that the flux rope is not formed even in the highly twisted model with a whole current-flowing model as shown in the middle panel.

Results for the relativistic treatment are given in Fig. 6. Formation of a flux rope is more evident in relativistic models. There is a sharp peak of $B_{\hat{\phi}}$ in the highly twisted state, irrespective of the current flow model. The configuration shown in the middle and right panels in Fig. 6 corresponds to the end point along a sequence of middle and right panels in Fig. 4. Among these highly twisted states shown in Figs. 5 and 6, there is no flux-rope structure only in the middle panel of Fig. 5. The model is also different in the energy increase ΔE considered in Figs. 3 and 4: $\Delta E_t > \Delta E_p$ in this model. In other models at the end point, we have $\Delta E_p > \Delta E_t$. The flux-rope contains a strong toroidal magnetic field, but a strong poloidal component is also needed to support the toroidal component. Thus, the flux-rope formation is associated with a significant structural change from a potential magnetic field in vacuum. This property is also numerically supported by previous research (Kojima 2017; Kojima & Okamoto 2018).

As inferred from Figs. 3 and 4, the flux-rope is associated in the upper branch. So the state is able to store more energy,

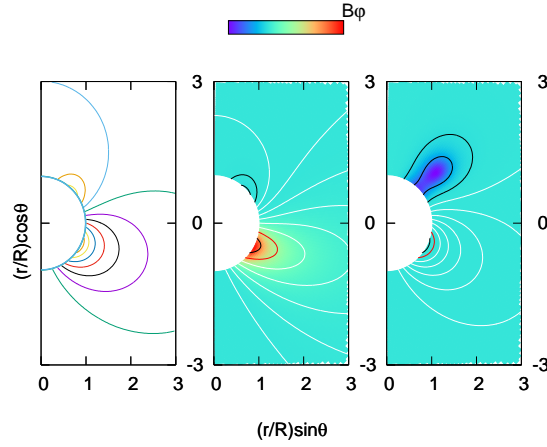


Figure 5. Contour lines of magnetic function G and color contour of $B_{\hat{\phi}}$ in the r - θ plane for a model with $a_2 = 1$ and $M/R = 0$. The left panel shows the potential field, and the middle panel shows the highly twisted state with a whole current-flowing model. The right panel shows results for a partially flowing model.

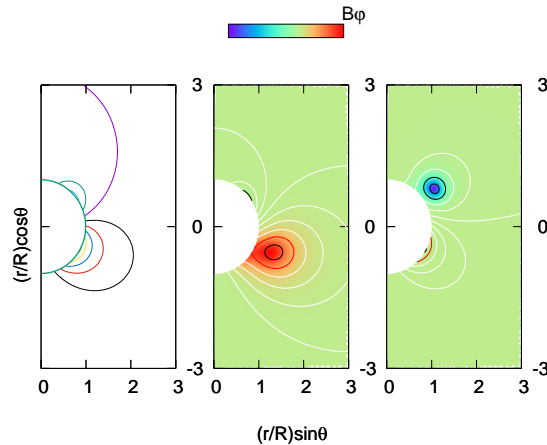


Figure 6. The same as Fig. 5, but for the model with a relativistic factor $M/R = 0.25$.

and may be meta-stable. Some elaborated methods are necessary to calculate such a state. There are some numerical results in which the flux rope is extended to several times the stellar radius, $r_c/R \sim 5$ in the models by [Pili et al. \(2015\)](#); [Akgün et al. \(2018\)](#). As an input parameter to construct a force-free magnetosphere, they fix the value of the critical radius r_c which is defined as the radial extent of the current flow region on the equatorial plane. Our results show that the location is not far from the central star. The center of the loops is within $r_c/R < 1.5$.

3.3 General relativistic confinement

In this subsection, we discuss the general relativistic effect on the flux rope formation. The effect is so far studied through numerical calculations. Here, we explain it by an interpretation of additional current j_g in a flat spacetime formulation, eq.(7). The 'general-relativity-induced current' j_g is not so large, and the ratio to true current $j_{\hat{\phi}}$ is $j_g/j_{\hat{\phi}} \sim 0.1$ in its magnitude. However, this small term is crucial in the exterior of a flux rope.

Figure 7 demonstrates the current distribution for $j_{\hat{\phi}}$ and j_g . The model corresponds to a highly twisted state for the

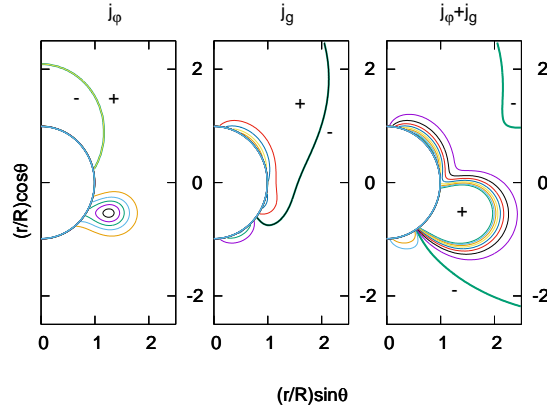


Figure 7. Contour azimuthal currents in eq.(7) for the model corresponding to the middle panel of Fig. 6. The thick curves denote the zero level, and the + or – symbols denote the sign of the current at these points. The left panel shows that $j_{\hat{\phi}}$ has a sharp peak at $(r/R, \theta) \approx (1.2, 120^\circ)$, which corresponds to the center of the flux rope in Fig. 6. The middle panel shows a ‘general-relativity-induced current’ j_g , which is in the opposite direction of $j_{\hat{\phi}}$ around each polar region. The right panel shows a sum of $j_{\hat{\phi}}$ and j_g . There is still a sharp peak around the center of each flux rope, but their higher level contours are omitted.

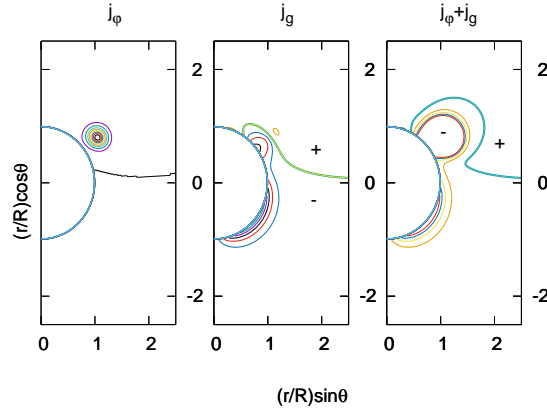


Figure 8. This figure reflects the same conditions as Fig.7, but for the model corresponding to the right panel of Fig. 6. A sharp peak of $j_{\hat{\phi}}$ at $(r/R, \theta) \approx (1.2, 60^\circ)$ in the left panel corresponds to the center of the flux rope in Fig. 6. In the right panel, there is still a sharp peak of $j_{\hat{\phi}} + j_g$ around the center of the flux rope, but their higher level contours are omitted.

whole current flowing model with $M/R = 0.25$ (middle panel of Fig. 6). There is a sharp maximum of $j_{\hat{\phi}} (> 0)$. The position corresponds to a center of the flux rope. In the distribution of $j_{\hat{\phi}} + j_g$ (right panel), the sharp peak-structure is still unchanged. However, the outer part is covered by an effectively negative current. This opposite current-flow supports the flux-rope formation. In Fig. 8, we also show another example for a partially current-flowing model with $M/R = 0.25$ (right panel of Fig. 6). In this case, there is a strong current $j_{\hat{\phi}} \leq 0$ in the northern hemisphere. The rope is surrounded with a positive current j_g produced by ‘gravity.’

In both models, the term j_g is in an opposite direction to the true current $j_{\hat{\phi}}$. The mechanism may be understood as follows. Supposed that a flux rope with $j_{\hat{\phi}} > 0$ is formed. The magnetic function G is a maximum in our model, and it outwardly decreases, i.e., $G_{,r} < 0$. Equation (8) provides $j_g < 0$ in the outer part of the rope. On the other hand, in the case of $j_{\hat{\phi}} < 0$, the center of the flux rope is the minimum of the magnetic function, and therefore $G_{,r} > 0$. Equation (8) provides

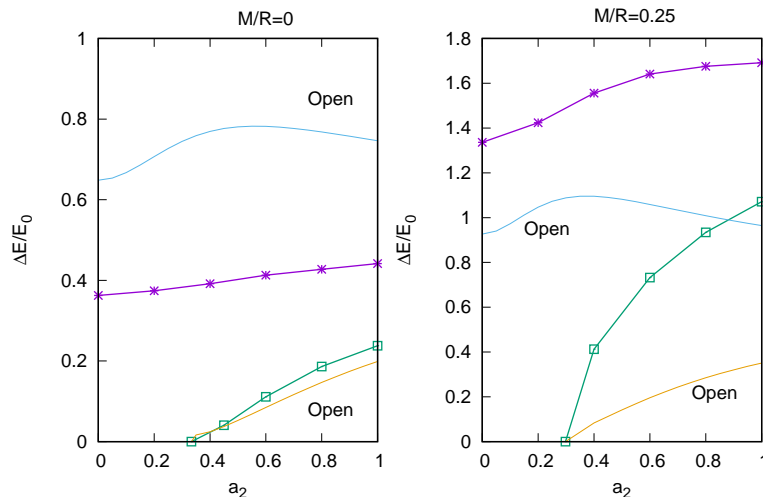


Figure 9. Maximum energy increment $\Delta E/E_0$ as a function of the quadrupole component a_2 . The left panel shows results with $M/R = 0$, while the right shows $M/R = 0.25$. Maximum energy with the whole current-flowing model is denoted by asterisks, and that with a partially current-flowing model is denoted by squares. The latter is possible for the range $a_2 > g_2/(3g_1) \approx 1/3$. A curve labeled 'open' denotes the partially open field energy $\Delta E_{\text{open}}/E_0 = (E_{\text{open}} - E_0)/E_0$.

$j_g > 0$ in the outer part. Whichever the direction of a current flow in the rope is, a counter-flow of effective current is produced in the exterior, and it holds the flux rope.

3.4 Energy

As shown in Figs. 3 and 4, the energy deposited in a magnetosphere increases with twisting for a given surface condition. Figure 9 shows the maximum increment $\Delta E_{\text{max}}/E_0 \equiv E_{\text{max}}/E_0 - 1$, as a function of a ratio a_2 , where $E_0 (= E_d + a_2^2 E_q)$ is the potential field energy. We also plot the energy difference $\Delta E_{\text{open}}/E_0 \equiv (E_{\text{open}} - E_0)/E_0$ between the partially open energy E_{open} and potential energy E_0 . Results with $M/R = 0$ are shown in the left panel. Both $\Delta E_{\text{max}}/E_0$ and $\Delta E_{\text{open}}/E_0$ are less sensitive to a_2 in the whole current flowing magnetosphere: $\Delta E_{\text{max}}/E_0 \sim 0.34\text{--}0.44$ and $\Delta E_{\text{open}}/E_0 \sim 0.66\text{--}0.78$ for $0 \leq a_2 \leq 1$. It is known that $\Delta E_{\text{max}}/E_0 = 0.34 < \Delta E_{\text{open}}/E_0 = 0.66$ with a purely dipole boundary in flat spacetime (Flyer et al. 2004). It is impossible that the maximum energy exceeds the open field energy even by including the quadrupole component in the flat model. The situation however changes, i.e., $E_{\text{max}} > E_{\text{open}}$ in the partially flowing model, which is relevant to $a_2 > 1/3$. The magnetic field configuration with a partially open energy E_{open} corresponds to the right panel in Fig. 2. The relevant energy is smaller than that shown in the middle panel, since the spatial region is limited. Figure 9 shows that ratios $\Delta E_{\text{max}}/E_0$ and $\Delta E_{\text{open}}/E_0$ monotonically increase with a_2 , since the current-flowing volume increases. The maximum energy is slightly larger than the open field energy, and the excess is approximately 10% ($E_{\text{max}} \approx 1.1 E_{\text{open}}$) in flat models.

Results in the framework of general relativity are given in the right panel of Fig. 9. The maximum excess $\Delta E_{\text{max}}/E_0$ ($\sim 1.34\text{--}1.69$) in a model with $M/R = 0.25$ is significantly larger than that in a model with $M/R = 0$. The large increase is closely related to the flux rope formation in a relativistic model (Kojima 2017; Kojima & Okamoto 2018). Furthermore, the maximum energy exceeds E_{open} in any model with $M/R = 0.25$. The excess is approximately 20–40% ($E_{\text{max}} \approx 1.2\text{--}1.4 E_{\text{open}}$). In the partially current-flowing model, fractional excess further increases by up to approximately 30–50% ($E_{\text{max}} \approx 1.3\text{--}1.5 E_{\text{open}}$). The energy in a magnetic field configuration containing an evident flux rope, as shown in Figs. 5 and 6, exceeds the open field energy. Substantial amount of energy is stored in the rope, and is likely to eject in dynamical transition.

4 DISCUSSION

In this paper, we have studied the energy storage in a relativistic force-free magnetosphere with a quadrupole component on the surface. The component is introduced to examine the effect of local irregularity of the magnetic fields, since a purely dipolar field is the ideal case, and higher multi-poles are likely to be involved on the magnetar surface. We calculated a sequence

of equilibrium models whose evolution may be characterized by increasing the helicity stored in the magnetosphere. The magnetic energy also increases along the sequence, and exceeds the open-field one in some cases. A state with $E_{\text{EM}} > E_{\text{open}}$ is regarded as a metastable state in its energetics. It may be changed to a lower energy state through an intermediate, open magnetic-field structure. During the transition, the magnetic flux rope, in which plasma is also contained, is ejected. This dynamical event may be related to an observed magnetar flare.

However, the amount of energy in the catastrophic transition is ambiguous, since it depends on the stability of higher energy states. That is, the excess $\Delta E = E_{\text{EM}} - E_{\text{open}}$ is almost zero when some kinds of instabilities set in soon after reaching a state with E_{open} . On the other hand, ΔE is further built up by remaining in a metastable state longer, and a huge amount of energy is possibly released. Such a transition requires a dynamical calculation for its solution (e.g., Li et al. 2012; Parfrey et al. 2013; Kojima & Kato 2014, as resistive simulation in flat spacetime), which is beyond the scope of the quasi-equilibrium approach used here.

We discuss the astrophysical observation. The energy-scale in most magnetar outbursts is not as large as the maximum stored in a dipolar magnetosphere, $E_{\text{EM}} \approx 0.1(B_p)^2 R^3 = 10^{46}(B_p/10^{14.5}\text{G})^2(R/12\text{km})^3$ erg. Here the energy is estimated in flat spacetime approximation using magnetic field strength B_p at the surface pole and stellar radius R . The general relativistic effect increases it by a factor 2-3. The outburst energy is $10^{41} - 10^{42}$ erg (Coti Zelati et al. 2018), such that the fraction is $\approx 10^{-4}$ (see footnote 2). Thus, the outburst is a small reconfiguration of the magnetic fields. One possibility to account for it is that the energy is not built up so much beyond a state with $\sim E_{\text{open}}$. The metastable state is likely to be destroyed. The second possibility is a structural change at a smaller scale. In this paper, we studied it by considering a locally twisted model with a limited current-flowing region. We considered current flow in a localized region produced by a quadrupole field. We found that the associated energy is naturally reduced, and that a state with $E_{\text{EM}} > E_{\text{open}}$ is possible irrespective of the spacetimes. In a flat treatment, the possibility for $E_{\text{EM}} > E_{\text{open}}$ is already explored (Wolfson et al. 2007, 2012). They found greater excess energy in the presence of an exterior potential field covering the non-potential field. In our models, which are different from theirs at some points, the maximum excess energy is 5% of the potential field energy in a flat spacetime. The value is significantly increased in a general relativistic model, up to 70%. The general relativistic effect confines the current flow in the vicinity of the star. The mechanism may be interpreted as a 'general-relativity-induced current,' which flows in a counter direction so as to cover a flux rope. The effect is also important for a globally twisted magnetosphere, when the flows are extended across the entire space.

The force-free approximation is also considered in the context of the pulsar magnetosphere, in which stellar rotation is more important; $|j| \ll \rho_{\text{GJC}} \sim \Omega B c$, where Ω is angular velocity. The model is recently examined in a general relativistic framework (Ruiz et al. 2014; Pétri 2016; Gralla et al. 2016, 2017). Compared with the estimate based on a flat spacetime treatment, total Poynting power increases by 20–60%. The general-relativistic effects are also studied in a vacuum electromagnetic field, exterior field of stationarily rotating or oscillating relativistic object in the literature (e.g., Muslimov & Tsygan 1986; Rezzolla et al. 2001; Kojima et al. 2004; Morozova et al. 2010; Pétri 2017, and the references therein); these researchers found that the general-relativistic correction is of the order $G_N M / (Rc^2) \sim 0.2 - 0.3$. The effects on a static twisted magnetosphere considered here and in previous publications (Kojima 2017; Kojima & Okamoto 2018) are found to be substantial, since a topological change of the magnetic field structures is associated. Outward eruption of magnetic flux is suppressed, and relativistic models are capable of storing significantly more energy than the corresponding potential field energy. Therefore, general relativistic effects will be taken into account in magnetar models. The stability and more detailed modeling remain for future research.

ACKNOWLEDGEMENTS

This work was supported by JSPS KAKENHI Grant Numbers JP26400276 and JP17H06361.

REFERENCES

- Akgün T., Miralles J. A., Pons J. A., Cerdá-Durán P., 2016, *MNRAS*, **462**, 1894
Akgün T., Cerdá-Durán P., Miralles J. A., Pons J. A., 2017, *MNRAS*, **472**, 3914
Akgün T., Cerdá-Durán P., Miralles J. A., Pons J. A., 2018, *MNRAS*, **474**, 625
Coti Zelati F., Rea N., Pons J. A., Campana S., Esposito P., 2018, *MNRAS*, **474**, 961
Flyer N., Fornberg B., Thomas S., Low B. C., 2004, *ApJ*, **606**, 1210
Fujisawa K., Kisaka S., 2014, *MNRAS*, **445**, 2777
Geppert U., Viganò D., 2014, *MNRAS*, **444**, 3198
Glampedakis K., Lander S. K., Andersson N., 2014, *MNRAS*, **437**, 2
Goldreich P., Reisenegger A., 1992, *ApJ*, **395**, 250

² In giant flares, the energies are scaled up to 10^{44} – 10^{46} ergs. The ratio is $\approx 10^{-2}$, since their sources (SGR 0526-66, SGR 1900+14, and SGR 1806-20) have somewhat stronger field strength $B_p = (5 - 20) \times 10^{14}\text{G}$ (Turolla et al. 2015)

- Gourgouliatos K. N., Cumming A., 2014, *MNRAS*, **438**, 1618
Gourgouliatos K. N., Wood T. S., Hollerbach R., 2016, *Proceedings of the National Academy of Science*, **113**, 3944
Gralla S. E., Lupsasca A., Philippov A., 2016, *ApJ*, **833**, 258
Gralla S. E., Lupsasca A., Philippov A., 2017, *ApJ*, **851**, 137
Hollerbach R., Rüdiger G., 2004, *MNRAS*, **347**, 1273
Kaspi V. M., Beloborodov A. M., 2017, *ARA&A*, **55**, 261
Kojima Y., 2017, *MNRAS*, **468**, 2011
Kojima Y., Kato Y. E., 2014, *Progress of Theoretical and Experimental Physics*, 2014, 023E01
Kojima Y., Kisaka S., 2012, *MNRAS*, **421**, 2722
Kojima Y., Okamoto S., 2018, *MNRAS*, **475**, 5290
Kojima Y., Matsunaga N., Okita T., 2004, *MNRAS*, **348**, 1388
Li J., Spitkovsky A., Tchekhovskoy A., 2012, *ApJ*, **746**, 60
Low B. C., Smith D. F., 1993, *ApJ*, **410**, 412
Morozova V. S., Ahmedov B. J., Zanotti O., 2010, *MNRAS*, **408**, 490
Muslimov A. G., Tsygan A. I., 1986, *Ap&SS*, **120**, 27
Parfrey K., Beloborodov A. M., Hui L., 2013, *ApJ*, **774**, 92
Pétri J., 2016, *MNRAS*, **455**, 3779
Pétri J., 2017, *MNRAS*, **472**, 3304
Pili A. G., Bucciantini N., Del Zanna L., 2015, *MNRAS*, **447**, 2821
Pili A. G., Bucciantini N., Del Zanna L., 2017, *MNRAS*, **470**, 2469
Rezzolla L., Ahmedov B. J., Miller J. C., 2001, *MNRAS*, **322**, 723
Ruiz M., Paschalidis V., Shapiro S. L., 2014, *Phys. Rev. D*, **89**, 084045
Turolla R., Zane S., Watts A. L., 2015, *Reports on Progress in Physics*, **78**, 116901
Viganò D., Rea N., Pons J. A., Perna R., Aguilera D. N., Miralles J. A., 2013, *MNRAS*, **434**, 123
Wolfson R., Larson J., Lionello R., 2007, *ApJ*, **660**, 1683
Wolfson R., Drake C., Kennedy M., 2012, *ApJ*, **750**, 25
Wood T. S., Hollerbach R., 2015, *Physical Review Letters*, **114**, 191101
Zhang M., Flyer N., Low B. C., 2006, *ApJ*, **644**, 575
Zhang M., Flyer N., Chye Low B., 2012, *ApJ*, **755**, 78